J Mol Model (2012) 18:2823–2829
DOI 10.1007/s00894-011-1298-7

ORIGINAL PAPER

Computational investigation of the effect of thermal perturbation on the mechanical unfolding of titin I27

Navneet Bung · U. Deva Priyakumar

Received: 13 June 2011 / Accepted: 2 November 2011 / Published online: 27 November 2011

Abstract The emergence of single-molecule force measurement experiments has facilitated a better understanding of protein folding pathways and the thermodynamics involved. Computational methods such as steered molecular dynamics (SMD) simulations are helpful in providing atomistic level information on the unfolding pathways. Recent experimental studies have showed that combinations of single-molecule experiments with traditional methods such as chemical and/or thermal denaturation yield additional insights into the folding phenomenon. In this study, we report results from extensive computations (a total of about 60 SMD simulations with a total length of about 0.4 μs) that address the effect of thermal perturbation on the mechanical stability of the I27 domain of the protein titin. A wide range of temperatures (280–340 K) were considered for the pulling, which was done at both constant velocity and constant force using SMD simulations. Good agreement with experimental data, such as for the trends in changes in average force and the maximum force with respect to the temperature, was obtained. This study identifies two competing pathways for the mechanical unfolding of I27, and illustrates the significance of combining various techniques to examine protein folding.

Keywords Protein folding · Steered molecular dynamics · Denaturation · Mechanical stability · Titin I27 · Folding pathways

Electronic supplementary material The online version of this article (doi:10.1007/s00894-011-1298-7) contains supplementary material, which is available to authorized users.

N. Bung · U. D. Priyakumar (✉)
Center for Computational Natural Sciences and Bioinformatics,
International Institute of Information Technology,
Hyderabad 500 032, India
e-mail: deva@iiit.ac.in

Introduction

During the past two decades or so, single-molecule force measurements using atomic force microscopy (AFM) have been extensively used to study protein folding [1–4]. Typically, a single molecule of the biomolecule under study is tethered between the AFM cantilever and its stage, and stretched at a known speed while simultaneously measuring the force. Similar methods have also been used to investigate RNA folding and aptamer–ligand binding [5–7]. Recently, the applicability of single-molecule experiments to investigations elucidating the biological activities of inhibitors and the design of new ligands has been demonstrated using SMD simulations [8]. These single-molecule manipulation techniques allow the characterization of not only the folded and unfolded states but also the intermediate states along the folding pathway [2]. The order parameter or the reaction coordinate for unfolding in these experiments is usually the distance between the terminal residues. However, the order parameter for protein folding is not necessarily this inter-residue distance. Hence, it is important to validate the applicability of these methods to study the structure-function relationships of a given biomolecule. Traditionally, chemical denaturants such as guanidinium chloride and thermal perturbation along with spectroscopic methods have been used to study protein folding [9]. Recent studies have shown that it is important to combine single-molecule experiments with either chemical denaturants or with thermal perturbations to study folding processes [10–14]. They proposed that such combinations of multiple techniques along with comparisons of results from multiple probes are useful for validating the protocol used [12]. Additionally, they provide an opportunity to explore various aspects of protein folding that may not be accessible by any of these methods

when used individually. Theoretical studies have already been performed to include temperature as a variable while investigating the mechanical stability of proteins and RNA [15–17].

Titin is a huge protein consisting of about 30,000 amino acids that has been shown to be crucial to the contraction and stretching of muscle [20]. The mechanical (un)folding of titin I27 has been extensively studied both experimentally, using single-molecule approaches [21–23], and computationally [24–31]. The structure of I27 consists of two sheets: β-strands A, B, E, and D form the first sheet, and β-strands A′, G, F, and C form the second sheet (Fig. 1). Schulten and coworkers have investigated the molecular level details of the force-induced unfolding of I27 using SMD simulations [24–26]. They have calculated force vs. extension profiles that are consistent with experimental data. They showed that the force peak observed at around 13 Å corresponds to the loss of interactions between the A and B and the A′ and G strands [24].

In the present study, we attempt to understand the effect of temperature on the mechanical unfolding of the titin I27 domain using SMD simulations. The protein was selected based on recent experimental studies of this protein [11, 13], and the validity of the end-to-end distance as the order parameter for the unfolding of this protein. Botello et al. showed that the free-energy barrier during the mechanical unfolding of I27 decreases linearly with respect to increasing temperature and the concentration of the chemical denaturant, guanidinium chloride [11]. A detailed study by Taniguchi et al. illustrated the effect of temperature on the mechanical stress of the native and intermediate states of I27 [13]. They hypothesized that the energy landscape does not alter with respect to temperature until the folded state reaches the intermediate state, although it changes substantially beyond that. The results obtained here are compared with the available experimental data, and the two show good agreement. Our results support the hypothesis for the energy landscape proposed by Taniguchi et al. [13], and show two competing unfolding pathways whose atomistic details are provided.

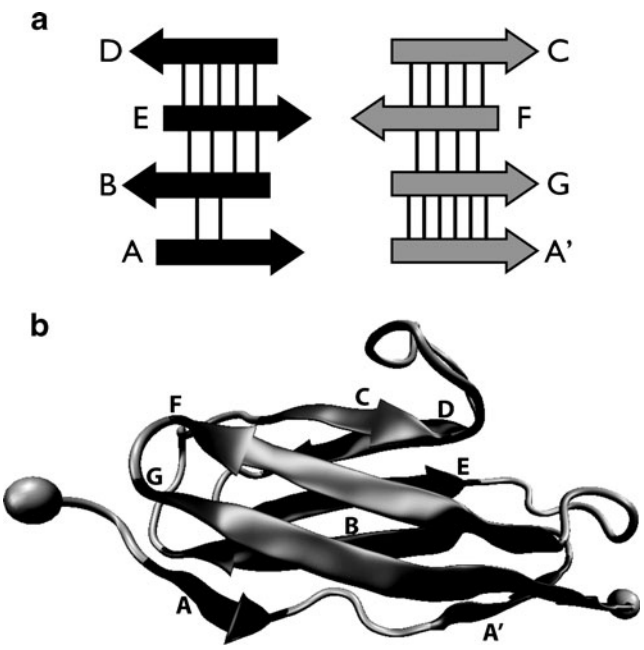

Fig. 1 **a** Secondary structure of titin I27. The two β-sheets are shown as *black and gray colored block arrows*, and the individual strands are named according to previous studies. **b** The tertiary structure of I27 (PDB ID: 1TIT) [18], rendered using the VMD program [19]. The β-strands are colored as in **a**, and the two spheres represent the N-terminal and C-terminal Cα atoms

Methods

The starting structure for the MD simulations was obtained from an earlier NMR study (PDB ID: 1TIT) [18]. All the MD simulations were performed using the NAMD biomolecular simulation program [32] using the CHARMM27 protein force field along with CMAP corrections [33, 34]. The simulations reported in the present paper were performed in an explicit solvent environment using the modified TIP3P water model. The simulation protocol used was based on previously published methods [26]. In short, the protein was solvated in pre-equilibrated water spheres of radius 35 Å. For the purpose of solvation, water spheres equilibrated at 280, 290, 300, 310, 320, 330, and 340 K were used, and the MD simulations were run at the corresponding temperatures. The systems thus solvated at different temperatures were subjected to 5000 steps of minimization followed by 100 ps of equilibration. During equilibration, the non-hydrogen atoms of the I27 domain were restrained using a mass-weighted harmonic constraint of 5 $kcalmol^{-1}Å^{-2}$. Constant temperature in these simulations was achieved using the Langevin method, and an integration time step of 1 fs was used. The nonbonded interactions were calculated with a distance cut-off of 10 Å, and zero was reached at 13 Å.

SMD simulations at constant velocity were carried out by fixing the Cα atom of the N-terminal residue (Leu-1) and applying external force to the Cα of the C-terminal residue (Leu-89). The forces were applied by restraining the Cα atom of the C-terminus to a restraint point along the line joining the N-terminal and C-terminal Cα atoms at a constant velocity of 0.1 $Åps^{-1}$. A spring constant (k) of 10 $kcalmol^{-1}Å^{-2}$ with an integration time of 1 fs was used in the constant-velocity SMD simulations. For a given value of k, the fluctuations in the position of the restrained atom are given by $\delta x \sim (k_b T/k)^{1/2}$. Thus, by selecting a very high value of k (stiff spring, 10 $kcalmolÅ^{-2}$), the fluctuations in the position of Cα of the C-terminal residue are of

the order of 0.24 Å at 280 K and 0.26 Å at 340 K. In contrast, the position fluctuations associated with a soft spring with low k values will be much larger [35]. However, it should be noted that the cantilever stiffness used in typical AFM experiments is about two orders of magnitude smaller than the stiffness due to the spring constant used here. Similar to this study, previous studies have used a similar stiff spring to account for the large fluctuations in the positions otherwise [26]. The SMD simulation for each system was continued until the protein formed the completely extended form that resulted in a rapid increase in the unfolding force. The SMD output, including the force vector and the coordinates of the C-terminal atom (i.e., the SMD atom), was saved every 10 fs. Five independent simulations with different sets of initial velocities were performed at each of the temperatures given above. An extra set of SMD simulations were carried out at four temperatures (280, 300, 320, and 340 K) and a lower velocity, 0.01 Åps^{-1}. Work done was calculated by integrating the forces as given by the following equation for each trajectory and averaging over the five trajectories at each temperature [36]:

$$W(t) = v \int_0^t dt\, f(t), \tag{1}$$

where v is the pulling velocity, $f(t)$ is the force required as a function of time to unfold the protein, and t is the time.

SMD simulations were also performed by fixing the N-terminus and applying a constant force of 750 pN to the Cα atom of the C-terminal residue in the direction of the line joining the two atoms. Similar to the constant-velocity SMD simulations, five independent simulations were carried out with different sets of initial velocities at four different temperatures (280, 300, 320, and 340 K). The error bars shown at each of the temperatures in the figures represent the standard error of the mean from the five independent observations. It should be noted that the estimates for the errors were calculated based on only five data points in each case, so they must be treated as rough estimates of the true errors. Overall, about 60 independent simulations were done that lasted for about 0.4 μs. The results obtained here are based on the simulations employing the CHARMM force field [33, 34]. All-atom CHARMM protein force field parameters have been shown to adequately represent the inter- and intramolecular forces in protein molecules in general [37]. However, it should be noted that these parameters were developed based on individual amino acids and small peptides, and benchmarked over a test set of proteins [38]. It was recently shown that even small errors in the potential energy functions tend to accumulate for large protein structures, and may result in not very accurate descriptions of the global minima [39]. This may be a crucial factor when using the potential energy functions in *ab initio* predictions of folded states.

Results and discussion

The present study was primarily motivated by recent experimental studies that employed a combination of

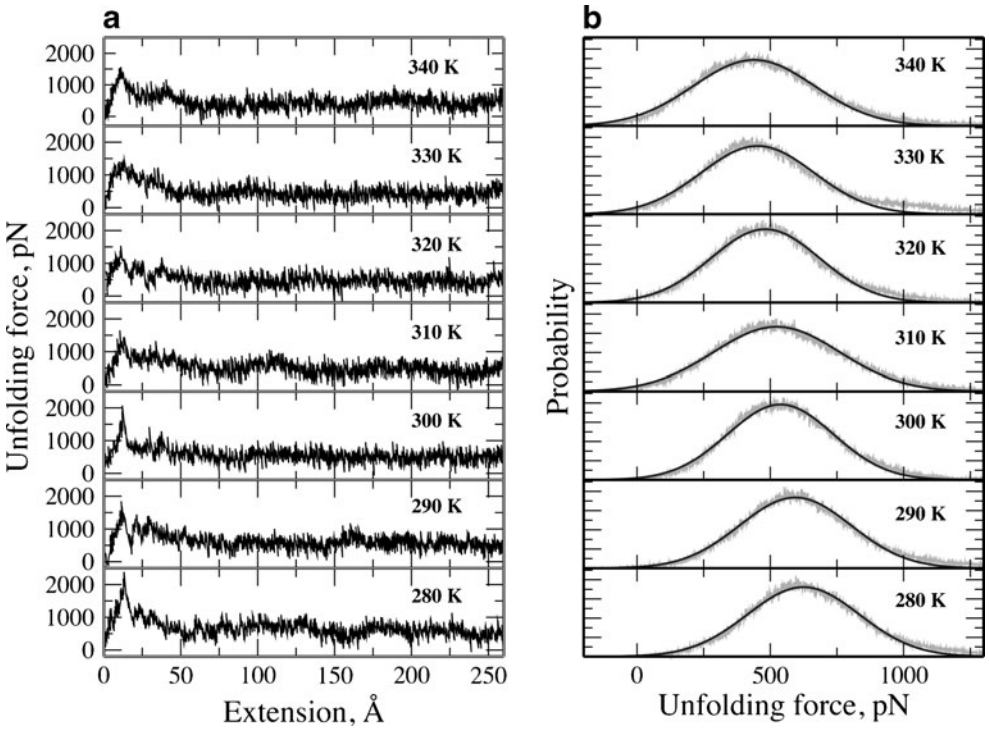

Fig. 2 **a** Force–extension profiles obtained from constant-velocity SMD simulations of I27 obtained at seven different temperatures. **b** Probability distributions of the unfolding forces (*gray lines*) obtained at the corresponding temperatures, including the curves fitted to Gaussian functions (*black lines*). Data from one of the five simulations at each temperature are given (see Figs. S1–S7 in the ESM)

mechanical unfolding using AFM along with thermal or chemical denaturation to study protein folding [11–13]. Here, we attempt to examine the importance of such studies to improve our understanding of protein folding by providing molecular level details of the effect of temperature on the mechanical unfolding of the titin I27 domain. In the current section, the differences in the unfolding of this protein at different temperatures, and their relevance to the experimental studies, are presented.

Force vs. extension profiles were obtained at different temperatures (280–340 K) using the constant-velocity SMD simulations. Select profiles from five independent simulations at each temperature are given in Fig. 2a (see Figs. S1–S7 in the "Electronic supplementary material," ESM, for all the data). The force–extension profiles obtained from the SMD simulations performed at the seven different temperatures were found to be qualitatively similar with respect to each other. However, quantitative differences in the magnitudes of the unfolding forces were observed. As noted before by Schulten and coworkers, the magnitudes of the forces obtained here are higher than those observed under experimental conditions due to the difference in the velocity at which the protein is extended [26]. The force vs. extension profiles were also obtained at a lower velocity (0.01 $Åps^{-1}$), and the qualitative trends obtained are similar to those obtained by Schulten and coworkers for a velocity of 1 $Åps^{-1}$, and for a velocity of 0.1 $Åps^{-1}$ (this work). Though the pulling speed used in the experiments is about six orders of magnitude less than the slowest velocity used here, similar results at the three different velocities indicate that the conclusions arrived at based on these results are possibly independent of the velocity in this range. It is not practical to perform the computations at a lower velocity. To examine the effect of temperature on the overall mechanical resistivity of the protein, probability distributions of the unfolding forces were computed (Fig. 2b, and Figs. S1–S7 in the ESM). All the histograms thus obtained follow a near-Gaussian distribution with properties that change with the temperature at which the MD simulations were performed. The probability distributions of the unfolding forces were fitted to Gaussian functions (Fig. 2b) using standard fitting tools.

The most probable unfolding force, the force at which the probability is maximum based on the Gaussian fit to the distribution, decreases linearly with increasing temperature (Fig. 3a). The values decrease from about 640 to about 425 pN for temperatures of 280 to 340 K. The results from the five independent SMD simulations performed at each of the seven temperatures studied here yielded similar results. The error bars shown at each of the temperatures in the figures represent the standard error of the mean based on five independent observations. This is in excellent agreement with a recent study by Botello et al., which showed that the peak position of the force distribution moves towards lower forces with increasing temperature [11]. Interestingly, while the unfolding forces are strongly dependent on the temperature, the simulations show that the extension at

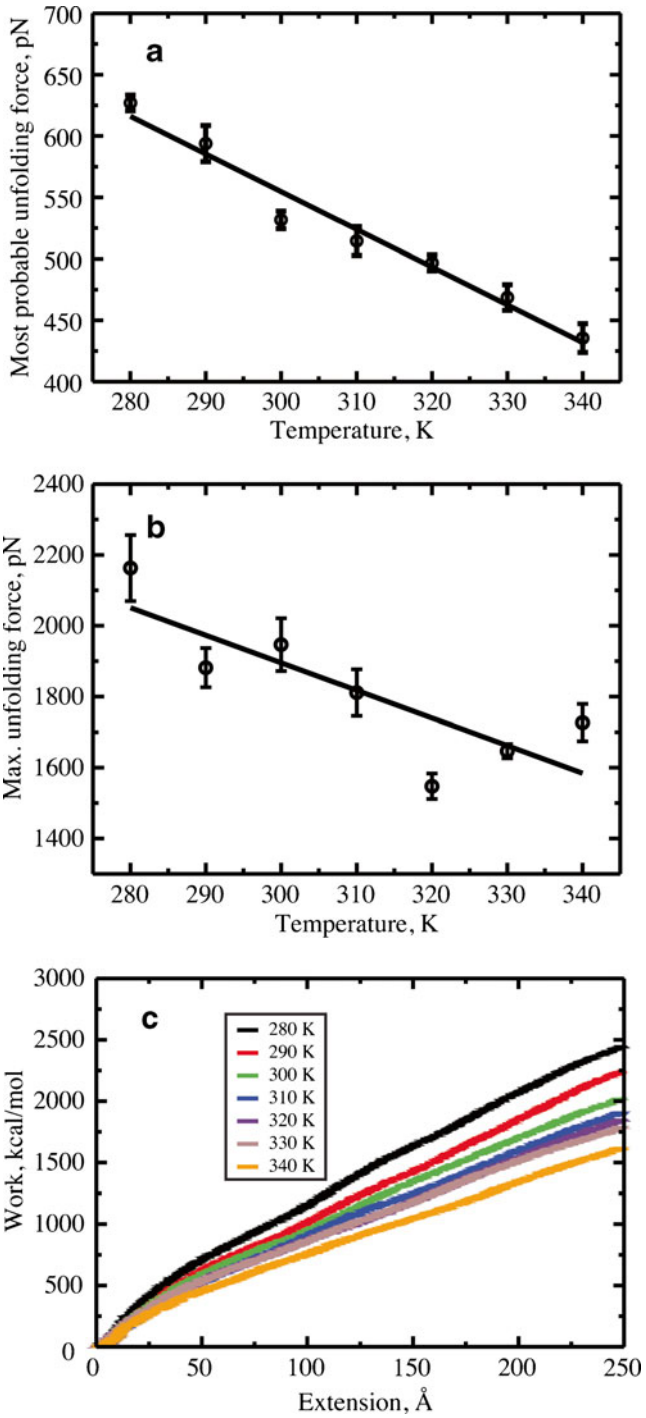

Fig. 3 **a** The change in the most probable unfolding force (force at the maximum probability) with temperature. The best possible linear fit is also given. **b** Peak force obtained from force–extension profiles attained at different temperatures, along with the linear fit. **c** Work vs. extension profiles obtained at different temperatures (K) using the constant velocity 0.1 $Åps^{-1}$

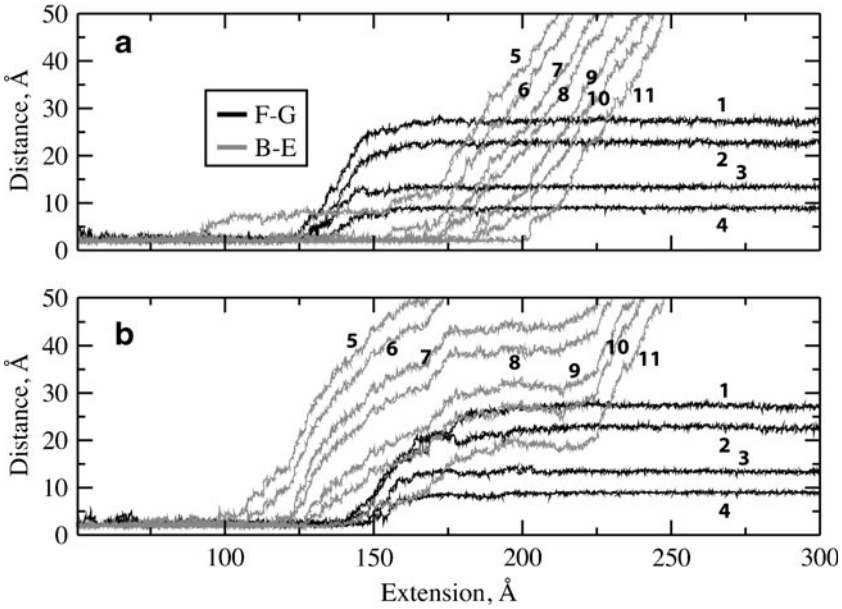

Fig. 4 Changes in the hydrogen bond donor–acceptor distances [*1* F73(N)–S80(O), *2* S80(N)–F73(O), *3* A75(N)–A78(O), *4* A78(N)–A75(O), *5* A19(N)–L60(O), *6* L60(N)–A19(O), *7* F21(N)–L58(O), *8* L58(N)–F21(O), *9* I23(N)–H56(O), *10* H56(N)–I23(O), and *11* L25(N)–K54(O)] between strands F and G (*black lines*) and B and E (*gray lines*), as calculated from two different trajectories that follow the two competing unfolding pathways. In **a**, FG unfolds before BE, and in **b**, BE unfolds before FG

which the maximum force is required during the unfolding process remains largely unchanged. The distance at which a peak is observed in each force-extension profile can be found in the range 10–13 Å at all temperatures (Fig. S8 in the ESM). Such a similarly positioned transition state in all of the simulations further validates the order parameter of end-to-end distance for the unfolding of I27. Substantial deviations would be expected if the order parameter for unfolding is not the same in thermal denaturation [40]. The present results indicate that the magnitude of the maximum force in the force–extension profiles varies with temperature (Fig. 3b). The unfolding force at the peak in the force–extension profile decreases approximately linearly with increasing temperature. Since the protein softens with increasing temperature, the force required to unfold the protein including the peak force decreases. Notable deviations are the maximum forces obtained at 320 and 340 K. The effect of temperature on the mechanical stability of titin I27, as discussed above, was further validated by another set of constant-velocity SMD simulations done at a lower velocity (0.01 Åps^{-1}) and at four temperatures (280, 300, 320, and 340 K). The trends for the changes in the average and the maximum forces of unfolding, and the extension at maximum force, were found to be consistent with the observations noted above.

The work done corresponding to protein unfolding was calculated by integrating the forces and averaging over the five different trajectories at each of the seven temperatures. Since the work done through extension depends on the pulling velocity, it is appropriate to compare the qualitative changes in the profiles with respect to temperature (Fig. 3c). The work profiles obtained at all seven temperatures at a pulling velocity of 0.1 Åps^{-1} are very similar up

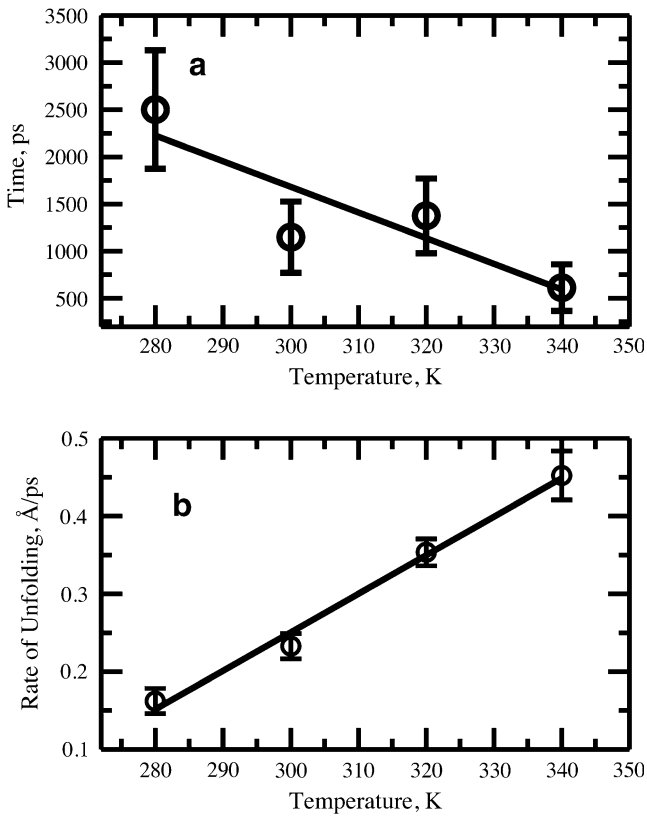

Fig. 5 **a** The time required to cross the barrier in constant-force pulling experiments decreases with increasing temperature. **b** Unfolding rates from constant-force SMD simulations—calculated from the slopes of extension–time profiles. Here, the unfolding rate corresponds to the rate after crossing the intermediate state on the way to the fully extended state. Each *error bar* represents the standard error of the mean calculated from five different runs at each temperature

to an extension of about 11 Å (approximately the position where the force required to unfold the protein is maximum). Beyond this extension, the work profiles show temperature dependency in the expected order, where the work required to extend the protein is larger at 280 K than at 340 K. Such an interesting change in the trend for the work required to unfold before and after 11 Å supports the hypothesis provided by Taniguchi et al. [13]. They proposed that the energy landscape remains similar with changes in temperature until the unfolding reaches the intermediate state (~9 Å), but it significantly changes after this extension. The work vs. extension profile for the complete range of extensions at the low velocity (0.01 Åps^{-1}) are given in the ESM (Fig. S9). The work profiles show similar trends at both velocities studied, especially in the range up to 50 Å, and are in agreement with the one proposed by Taniguchi et al.

The unfolding pathways that occur for I27 under all conditions (different temperatures and different velocities) were compared with each other and with previously published studies. As observed in earlier studies, the intramolecular interactions between the A′ and G strands were found to require a larger force than the others. Initially, the hydrogen bonds between A and B and then A′ and G are lost within about 14 Å of extension. The last set of interactions to be disrupted are the hydrogen bonds between the E and D β-strands. However, the order in which the intramolecular interactions between the B and E, F and G, and F and C strands are distorted was found to follow two distinct patterns. The donor–acceptor distances corresponding to the hydrogen bonding between the two pairs of strands obtained from two different trajectories that show different unfolding pathways are given in Fig. 4. In some of the SMD simulations, F–G contacts were found to distort first, followed by B–E contacts accompanied by F–C interactions (Fig. 4a). In the others, B–E strands were found to unfold first, followed by F–G and F–C (Fig. 4b). Results from all of the constant-velocity simulations are provided in Figs. S10–S16 in the ESM. The consistent observation of two different unfolding patterns for the titin I27 domain (as shown in the figure) indicates two competing pathways. It should, however, be noted that the unfolding of the B, E, F, and C β-strands occurs after the unfolding transition state. Notably, such competing pathways have not been reported from previous computational or experimental approaches.

The results discussed above were further validated by performing constant-force (750 pN) SMD simulations at four different temperatures. The unfolding pathways obtained are consistent with the discussion above. From the extension vs. time profiles (Fig. S17), the time required to cross the transition state barrier in each simulation was calculated. This time was found to linearly decrease with increasing temperature (Fig. 5a), consistent with the above discussion. The extension vs. time profiles obtained at different temperatures were qualitatively similar, indicating that the distance between the terminal residues is a reasonable order parameter for the unfolding of I27, even under thermal denaturation conditions. The rates of unfolding at constant force after the barrier had been crossed were also calculated, and were found to increase linearly with increasing temperature (Fig. 5 b).

Summary

In summary, the current study reports the effect of thermal perturbation on the mechanical stability of the I27 domain of the protein titin using constant-velocity and constant-force SMD simulations. The average and maximum unfolding forces obtained from the constant-velocity simulations show linear relationships with temperature. Work vs. extension profiles calculated at different temperatures show that the energy landscape corresponding to protein unfolding does not alter with temperature (within the temperature range considered here) until it reaches the intermediate state, but they shows different behavior after crossing the transition state, supporting a recent hypothesis based on an experimental study. The study also identifies hitherto unknown competing pathways for the unfolding of I27. Combining forced pulling along with thermal denaturation to examine protein folding is proposed as a powerful tool, especially in cases where the order parameter for unfolding is not simply the distance between the terminal residues [40]. We are currently investigating such changes in the unfolding pathways of proteins when the order parameter of end-to-end distance is not valid.

Acknowledgments UDP thanks the Department of Biotechnology (DBT), Govt. of India, for the Innovative Young Biotechnologist Award. We acknowledge DBT for financial assistance (BT/03/IYBA/2010).

References

1. Forman JR, Clarke J (2007) Mechanical unfolding of proteins: insights into biology, structure and folding. Curr Opin Struct Biol 17:58–66
2. Kumar S, Li MS (2010) Biomolecules under mechanical force. Phys Rep 486:1–74
3. Best RB, Clarke J (2002) What can atomic force microscopy tell us about protein folding? Chem Commun 183–193
4. Bustamante C, Chemla YR, Forde NR, Izhaky D (2004) Mechanical processes in biochemistry. Annu Rev Biochem 73:705–748
5. Greenleaf WJ, Frieda KL, Foster DAN, Woodside MT, Block SM (2008) Direct observation of hierarchical folding in single riboswitch aptamers. Science 319:630–633
6. Li PTX, Vieregg J, Tinoco I Jr (2008) How RNA unfolds and refolds. Annu Rev Biochem 77:77–100
7. Hyeon C, Morrison G, Thirumalai D (2008) Force-dependent hopping rates of RNA hairpins can be estimated from accurate

measurement of the folding landscapes. Proc Natl Acad Sci USA 105:9604–9609
8. Colizzi F, Perozzo R, Scapozza L, Recanatini M, Cavalli A (2010) Single-molecule pulling simulations can discern active from inactive enzyme inhibitors. J Am Chem Soc 132:7361–7371
9. Dobson CM, Šali A, Karplus M (1998) Protein folding: a perspective from theory and experiment. Angew Chem Int Ed 37:868–893
10. Carrion-Vazquez M, Oberhauser AF, Fowler SB, Marszalek PE, Broedel SE, Clarke J, Fernandez JM (1999) Mechanical and chemical unfolding of a single protein: a comparison. Proc Natl Acad Sci USA 96:3694–3699
11. Botello E, Harris NC, Sargent J, Chen WH, Lin KJ, Kiang CH (2009) Temperature and chemical denaturant dependence of forced unfolding of titin i27. J Phys Chem B 113:10845–10848
12. Cao Y, Li H (2008) How do chemical denaturants affect the mechanical folding and unfolding of proteins? J Mol Biol 375:316–324
13. Taniguchi Y, Brockwell DJ, Kawakami M (2008) The effect of temperature on mechanical resistance of the native and intermediate states of I27. Biophys J 95:5296–5305
14. Schlierf M, Rief M (2005) Temperature softening of a protein in single-molecule experiments. J Mol Biol 354:497–503
15. Hyeon C, Thirumalai D (2003) Can energy landscape roughness of proteins and RNA be measured by using mechanical unfolding experiments? Proc Natl Acad Sci USA 100:10249–10253
16. Klimov D, Thirumalai D (1999) Stretching single-domain proteins: phase diagram and kinetics of force-induced unfolding. Proc Natl Acad Sci USA 96:6166–6170
17. Isralewitz B, Gao M, Schulten K (2001) Steered molecular dynamics and mechanical functions of proteins. Curr Opin Struct Biol 11:224–230
18. Improta S, Politou AS, Pastore A (1996) Immunoglobulin-like modules from titin I-band: extensible components of muscle elasticity. Structure 4:323–337
19. Humphrey W, Dalke A, Schulten K (1996) VMD: Visual Molecular Dynamics. J Mol Graph 14:33–38
20. Labeit S, Kolmerer B, Linke WA (1997) The giant protein titin: emerging roles in physiology and pathophysiology. Circul Res 80:290–294
21. Rief M, Gautel M, Oesterhelt F, Fernandez JM, Gaub HE (1997) Reversible unfolding of individual titin immunoglobulin domains by AFM. Science 276:1109–1112
22. Kellermayer MSZ, Smith SB, Granzier HL, Bustamante C (1997) Folding–unfolding transitions in single titin molecules characterized with laser tweezers. Science 276:1112–1116
23. Tskhovrebova L, Trinick J, Sleep J, Simmons R (1997) Elasticity and unfolding of single molecules of the giant muscle protein titin. Nature 387:308–312
24. Lu H, Schulten K (2000) The key event in force-induced unfolding of titin's immunoglobulin domains. Biophys J 79:51–65
25. Lu H, Schulten K (1999) Steered molecular dynamics simulation of conformational changes of immunoglobulin domain I27 interpret atomic force microscopy observations. Chem Phys 247:141–153
26. Lu H, Isralewitz B, Krammer A, Vogel V, Schulten K (1998) Unfolding of titin immunoglobulin domains by steered molecular dynamics simulation. Biophys J 75:662–671
27. Fowler SB, Best RB, Toca Herrera JL, Rutherford TJ, Steward A, Paci E, Karplus M, Clarke J (2002) Mechanical unfolding of a titin Ig domain: structure of unfolding intermediate revealed by combining AFM, molecular dynamics simulations, NMR and protein engineering. J Mol Biol 322:841–849
28. Cieplak M, Hoang TX, Robbins MO (2002) Folding and stretching in a Go like model of titin. Proteins Struct Funct Bioinf 49:114–124
29. Ho BK, Agard DA (2010) An improved strategy for generating forces in steered molecular dynamics: the mechanical unfolding of titin, e2lip3 and ubiquitin. PloS one 5:e13068
30. Li PC, Makarov DE (2003) Theoretical studies of the mechanical unfolding of the muscle protein titin: bridging the time-scale gap between simulation and experiment. J Chem Phys 119:9260–9268
31. Li MS, Gabovich A, Voitenko A (2008) New method for deciphering free energy landscape of three-state proteins. J Chem Phys 129:105102
32. Phillips JC, Braun R, Wang W, Gumbart J, Tajkhorshid E, Villa E, Chipot C, Skeel RD, Kale L, Schulten K (2005) Scalable molecular dynamics with NAMD. J Comput Chem 26:1781–1802
33. Mackerell AD, Feig M, Brooks CL (2004) Extending the treatment of backbone energetics in protein force fields: limitations of gas-phase quantum mechanics in reproducing protein conformational distributions in molecular dynamics simulations. J Comput Chem 25:1400–1415
34. MacKerell AD, Bashford D, Bellott DRL, Evanseck JD, Field MJ, Fischer S, Gao J, Guo H, Ha S, Joseph-McCarthy D, Kuchnir L, Kuczera K, Lau FTK, Mattos C, Michnick S, Ngo T, Nguyen DT, Prodhom B, Reiher WE, Roux B, Schlenkrich M, Smith JC, Stote R, Straub J, Watanabe M, Wiorkiewicz-Kuczera J, Yin D, Karplus M (1998) All-atom empirical potential for molecular modeling and dynamics studies of proteins. J Phys Chem B 102:3586–3616
35. Izrailev S, Stepaniants S, Isralewitz B, Kosztin D, Lu H, Molnar F, Wriggers W, Schulten K (1999) Steered molecular dynamics. In: Deuflhard P, Hermans J, Leimkuhler B, Mark A, Skeel RD, Reich S (eds) Computational molecular dynamics: challenges, methods, ideas. Springer, Berlin, 4:39–65
36. Balsera M, Stepaniants S, Izrailev S, Oono Y, Schulten K (1997) Reconstructing potential energy functions from simulated force-induced unbinding processes. Biophys J 73:1281–1287
37. Rueda M, Ferrer-Costa C, Meyer T, Pèrez A, Camps J (2007) A consensus view of protein dynamics. Proc Natl Acad Sci USA 104:796–801
38. Mackerell A (2004) Empirical force fields for biological macromolecules: overview and issues. J Comput Chem 25:1584–1604
39. Faver JC, Benson ML, He X, Roberts BP, Wang B, Marshall MS, Sherrill CD, Merz Jr KM (2011) The energy computation paradox and ab initio protein folding. PloS one 6:e18868
40. Law R, Liao G, Harper S, Yang G, Speicher DW, Discher DE (2003) Pathway shifts and thermal softening in temperature-coupled forced unfolding of spectrin domains. Biophys J 85:3286–3293